

This is the accepted manuscript made available via CHORUS. The article has been published as:

## Epitaxial SrTiO<sub>3</sub> film on silicon with narrow rocking curve despite huge defect density

Z. Wang, B. H. Goodge, D. J. Baek, M. J. Zachman, X. Huang, X. Bai, C. M. Brooks, H. Paik, A. B. Mei, J. D. Brock, J-P. Maria, L. F. Kourkoutis, and D. G. Schlom

Phys. Rev. Materials **3**, 073403 — Published 29 July 2019

DOI: [10.1103/PhysRevMaterials.3.073403](https://doi.org/10.1103/PhysRevMaterials.3.073403)

# Epitaxial SrTiO<sub>3</sub> Film on Silicon with Narrow Rocking Curve Despite Huge Defect Density

Z. Wang,<sup>1,2</sup> B. H. Goodge,<sup>1,3</sup> D. J. Baek,<sup>4</sup> M. J. Zachman,<sup>1, b)</sup> X. Huang,<sup>5</sup> X. Bai,<sup>1</sup> C. M. Brooks,<sup>2</sup> H. Paik,<sup>2</sup> A. B. Mei,<sup>2</sup> J. D. Brock,<sup>1,5</sup> J. P. Maria,<sup>6</sup> L. F. Kourkoutis,<sup>1,3</sup> and D. G. Schlom<sup>2,3,a)</sup>

<sup>1</sup>*School of Applied and Engineering Physics, Cornell University, Ithaca, NY, 14853, USA*

<sup>2</sup>*Department of Materials Science and Engineering, Cornell University, Ithaca, NY, 14853, USA*

<sup>3</sup>*Kavli Institute at Cornell for Nanoscale Science, Ithaca, NY, 14853, USA*

<sup>4</sup>*School of Electrical and Computer Engineering, Cornell University, Ithaca, NY 14853, USA*

<sup>5</sup>*Cornell High Energy Synchrotron Source, Cornell University, Ithaca, NY, 14853, USA*

<sup>6</sup>*Department of Materials Science, North Carolina State University, Raleigh, North Carolina, 27695, USA*

The structural perfection and defect microstructure of epitaxial (001) SrTiO<sub>3</sub> films grown on (001) Si was assessed by a combination of x-ray diffraction and scanning transmission electron microscopy. Conditions were identified that yield 002 SrTiO<sub>3</sub> rocking curves with full width at half maximum below 0.03° for films ranging from 2-300 nm thick, but this is because this particular peak is insensitive to the  $\sim 8 \times 10^{11} \text{ cm}^{-2}$  density of threading dislocations with pure edge character and extended defects containing dislocations and out-of-phase boundaries. Our results show that one narrow rocking curve peak is insufficient to characterize the structural perfection of epitaxial films.

The integration of functional oxides with the backbone of semiconductor technology, silicon, has the potential to make the exceptional functional properties of oxides and oxide interfaces available in mainstream semiconductor devices. Many functional oxides have the

---

a) Author to whom correspondence should be addressed. Electronic mail: [schlom@cornell.edu](mailto:schlom@cornell.edu).

b) Current address: Center for Nanophase Materials Sciences, Oak Ridge National Laboratory, Oak Ridge, TN 37831, USA

perovskite structure and the ability to epitaxially integrate SrTiO<sub>3</sub>, one of the most widely used substrates for the epitaxial growth of functional oxides, directly on (001) Si [1] provides a gateway to the functionalities of perovskite oxides on silicon [2]. Though SrTiO<sub>3</sub> turned out to be unsuitable as a high-dielectric-constant alternative gate oxide on silicon due to its small conduction band offset [3], SrTiO<sub>3</sub>-templated silicon offers a sound platform for integrating the unique properties of functional oxides with silicon.

Examples of the phenomena and functional properties that have been achieved on SrTiO<sub>3</sub>-buffered silicon include: ferroelectricity utilizing Pb(Zr,Ti)O<sub>3</sub> [4, 5] and ultrathin SrTiO<sub>3</sub> [6], ferromagnetism utilizing La<sub>0.7</sub>Sr<sub>0.3</sub>MnO<sub>3</sub> [7, 8], multiferroicity utilizing BiFeO<sub>3</sub> [9], piezoelectricity utilizing Pb(Mg<sub>1/3</sub>Nb<sub>2/3</sub>)O<sub>3</sub>-PbTiO<sub>3</sub> (PMN-PT) [10], flexoelectricity utilizing SrTiO<sub>3</sub> [11], superconductivity utilizing YbBa<sub>2</sub>Cu<sub>3</sub>O<sub>7-x</sub> [12], electro-optical properties utilizing BaTiO<sub>3</sub> [13], two-dimensional electron gases utilizing the LaAlO<sub>3</sub>/SrTiO<sub>3</sub> interface [14] and LaTiO<sub>3</sub>/SrTiO<sub>3</sub> interface [15], and the photocatalysis of water reduction utilizing a thin epitaxial SrTiO<sub>3</sub> protection layer [16]. Thanks to the well developed Czochralski method of growing large-scale silicon single crystals, growing SrTiO<sub>3</sub> on silicon also enhances scalability to large diameter substrates [17, 18]. This is in contrast with the growth on SrTiO<sub>3</sub> single crystal substrates which are currently restricted by the diameter of high quality SrTiO<sub>3</sub> at or below 2 inches [19]. The ability of epitaxial SrTiO<sub>3</sub>-on-silicon to facilitate the jump to large substrates—provided the SrTiO<sub>3</sub> layer has sufficient structural perfection—could be game-changing for oxide electronics, paving a way to industrialize multi-functional thin films for devices.

Various techniques have been employed in growing SrTiO<sub>3</sub> films on silicon, including thermal evaporation [1], molecular-beam epitaxy (MBE) [20-24], and pulsed-laser deposition (PLD) [25]. Among these techniques, MBE is the most reliable for growing epitaxial SrTiO<sub>3</sub>

films on silicon [26-28], thanks to its ultra-high vacuum environment, exquisite control of atomic layering, and gentle growth conditions (the kinetic energy of the supplied species are all  $<1$  eV).

A key step in the growth of epitaxial  $\text{SrTiO}_3$  thin films on silicon is to deposit a submonolayer of strontium metal on the silicon substrate prior to the growth of  $\text{SrTiO}_3$  [1, 20, 21, 24]. The optimal dosage on a clean (001) Si surface is a half a monolayer [29]. It is widely recognized that this submonolayer of strontium metal is essential to the epitaxial growth of  $\text{SrTiO}_3$  on silicon [20, 24, 27, 29, 30], and it may play a role in the phase-separation instability of 1 nm thick  $\text{SrTiO}_3$  on silicon [31]. An important question, which has not been systematically studied, is the influence of the deposition temperature of this half a monolayer of strontium on the growth of  $\text{SrTiO}_3$  films on silicon, especially with regard to the crystalline quality of the  $\text{SrTiO}_3$  film. It has been shown that the deposition temperature of the submonolayer of strontium metal can influence the crystalline quality of epitaxial BaO films grown on silicon [32]; but there are no quantitative investigations of the influence of the deposition temperature of the half a monolayer of strontium on the crystalline perfection of  $\text{SrTiO}_3$  films on silicon.

In this Letter we study the effect of the deposition temperature of the initial half monolayer of strontium metal on silicon on the x-ray diffraction (XRD) rocking curves ( $\omega$  scans) of the 002  $\text{SrTiO}_3$  peaks. Narrow XRD rocking curves are usually considered synonymous with high structural quality [33, 34]. Our results indicate that when the half a monolayer of strontium is deposited at substrate temperatures in the 200-800 °C range,  $\text{SrTiO}_3$  films on silicon with a rocking curve full width at half maximum (FWHM) of the 002  $\text{SrTiO}_3$  peak comparable to that of typical  $\text{SrTiO}_3$  single crystals [35-38] can be achieved for films over the entire range of film thickness studied (2 – 300 nm). Despite the record narrow FWHM of the 002  $\text{SrTiO}_3$  rocking curve, measuring XRD  $\phi$  scans of the 101  $\text{SrTiO}_3$  peaks in the same films reveals that

significantly greater disorder is found to exist in-plane than out-of-plane. To characterize the defect microstructure in these SrTiO<sub>3</sub> films in greater detail, atomic resolution scanning transmission electron microscopy (STEM) reveals a threading dislocation density about six orders of magnitude *higher* than typical SrTiO<sub>3</sub> single crystals [39-41]. Thus, we conclude that a single narrow rocking curve peak is insufficient to characterize the structural perfection of epitaxial films.

All SrTiO<sub>3</sub> films in this study were grown in a Veeco GEN10 system on commercial three-inch-diameter (001) Si wafers. Elemental strontium and titanium beams were evaporated from a conventional low-temperature effusion cell and a Ti-Ball [42], respectively. Molecular oxygen was introduced and controlled via a piezoelectric leak valve. The temperature of the silicon substrate was monitored with either an optical pyrometer with a measurement wavelength of 980 nm (for substrate temperatures above 500 °C) or a thermocouple (for substrate temperatures below 500 °C). *In-situ* reflection high-energy electron diffraction (RHEED) was used to monitor the growth. The crystalline perfection of the SrTiO<sub>3</sub> films was assessed *ex situ* by XRD  $\theta$ -2 $\theta$ , rocking curve ( $\omega$  scans), and  $\phi$  scans, using either a Rigaku SmartLab or a PANalytical X'pert system with Cu  $K_{\alpha 1}$  radiation. The film microstructure was characterized by STEM using an aberration corrected FEI Titan Themis 300 operated at 300 keV.

Prior to the growth of each SrTiO<sub>3</sub> film, the strontium and titanium fluxes were precisely matched at  $\sim 10^{13}$  atoms·cm<sup>-2</sup>·s<sup>-1</sup> via a combined shuttered and codeposition RHEED calibration method [6, 43, 44]. The silicon substrate was cleaned in an ultraviolet ozone cleaner for  $\sim 20$  min to remove organic contamination, before being loaded into the MBE growth chamber with a base pressure in the high 10<sup>-9</sup> Torr range. The native surface SiO<sub>2</sub> of the silicon substrate was removed by heating the silicon substrate to  $\sim 980$  °C in ultrahigh vacuum for  $\sim 20$  min. Next, the clean

silicon surface was dosed with a half of a monolayer of strontium ( $3.4 \times 10^{14}$  atoms·cm<sup>-2</sup>) at substrate temperatures ranging from ~200 to ~850 °C; at high temperature not all of the incident strontium remained on the substrate surface. Finally, the substrate was cooled down to 200-300 °C for the growth of the SrTiO<sub>3</sub> film. This is the most challenging part of the growth process [21].

One of the difficulties of growing SrTiO<sub>3</sub> films on silicon is the initiation of the SrTiO<sub>3</sub> growth, where oxygen should be introduced into the chamber to oxidize strontium and titanium atoms to form SrTiO<sub>3</sub>, yet the silicon surface should be protected from oxygen to avoid forming an amorphous SiO<sub>2</sub> layer that precludes epitaxial growth. Several methodologies have been described to initiate the growth of SrTiO<sub>3</sub> on silicon. The crystalline quality of the resulting SrTiO<sub>3</sub> films on silicon vary significantly from method to method. In one method, after depositing the submonolayer strontium, this submonolayer strontium is exposed to oxygen prior to the deposition of the SrTiO<sub>3</sub> film [45-47]. In another method SrO and TiO<sub>2</sub> layers are deposited at a sufficiently low substrate temperature that they are initially amorphous and then during a subsequent vacuum annealing step are recrystallized into SrTiO<sub>3</sub> [15, 24, 26]. For the method we use in this study, the SrTiO<sub>3</sub> film is grown by codepositing (strontium, titanium, and oxygen are all supplied simultaneously) 2.5 unit cells of SrTiO<sub>3</sub> at a temperature below 300 °C (but sufficiently warm that the deposited layers remain crystalline) without previously exposing the submonolayer strontium to oxygen. While the principle of the growth follows the epitaxy-by-periodic-annealing method [21], great care is taken at the stage when oxygen is introduced into the vacuum chamber.

To be specific, the strontium and titanium shutters are kept closed as the oxygen is first introduced and the background oxygen pressure ramps up. When the oxygen partial pressure reaches  $\sim 5 \times 10^{-9}$  Torr, the strontium and titanium shutters are opened simultaneously as the

oxygen partial pressure slowly makes its way to  $(5 - 7) \times 10^{-8}$  Torr. The proper ramping rate of this oxygen initiation process is key for growing  $\text{SrTiO}_3$  films of relatively high crystalline quality on silicon [21, 48]. If the strontium and titanium shutters are opened too early before the oxygen partial pressure reaches  $\sim 5 \times 10^{-9}$  Torr, or the shutters are opened too late when a considerable amount of oxygen (with oxygen partial pressure much larger than  $5 \times 10^{-9}$  Torr) is already established in the chamber, the crystalline quality of the  $\text{SrTiO}_3$  film is severely degraded. Following the growth of the 2.5 unit-cell-thick  $\text{SrTiO}_3$  layer, the oxygen valve is closed and the remaining oxygen is pumped out of the chamber to an oxygen partial pressure below  $\sim 1 \times 10^{-9}$  Torr. The 2.5 unit-cell-thick  $\text{SrTiO}_3$  film is then annealed at  $\sim 580^\circ\text{C}$  for  $\sim 8$  min in vacuum to enhance its crystalline quality, before being cooled down to  $\sim 300^\circ\text{C}$  for the deposition of an additional 2.5 unit-cell-thick  $\text{SrTiO}_3$  layer. For the growth of the second 2.5 unit-cell-thick  $\text{SrTiO}_3$  layer, the strontium and titanium shutters do not necessarily need to be opened immediately after the oxygen partial pressure reaches  $5 \times 10^{-9}$  Torr because the first 2.5 unit-cells of  $\text{SrTiO}_3$  serves as an oxygen diffusion barrier and helps to protect the silicon substrate from being oxidized.

A schematic of the growth parameters used for the first and the second 2.5 unit-cell-thick  $\text{SrTiO}_3$  layers, as well as one set of actual growth parameters (substrate temperature and oxygen partial pressure) are shown in Figs. 1(a) and 1(b), respectively. This epitaxy-by-periodic-annealing method was repeated three times to achieve a total  $\text{SrTiO}_3$  film thickness of 7.5 unit cells. Upon this  $\text{SrTiO}_3$  buffer layer additional  $\text{SrTiO}_3$  was grown by codeposition at a temperature of  $\sim 580^\circ\text{C}$  and an oxygen partial pressure of  $\sim (5 - 7) \times 10^{-8}$  Torr.

$\text{SrTiO}_3$  films on silicon with total thickness ranging from 2 – 300 nm were grown using the meticulously controlled growth pathway described above. Figure 2 shows RHEED images at

different growth stages from a 20 nm thick SrTiO<sub>3</sub> film. These RHEED images are from the same sample for which the growth parameters are shown in Fig. 1(b). No other phases were detected in the RHEED patterns; the 20 nm thick SrTiO<sub>3</sub> film was epitaxial and single-phase. The sharp and streaky RHEED patterns indicate that the surface of the SrTiO<sub>3</sub> film is smooth.

Figure 3(a) shows the XRD  $\theta$ - $2\theta$  scan of the same 20 nm thick SrTiO<sub>3</sub> film on silicon. The presence of only  $00\ell$  Bragg reflections in combination with the RHEED patterns in Fig. 2 show that the as-grown SrTiO<sub>3</sub> film is epitaxial. Figure 3(b) shows the corresponding rocking curve of the 002 SrTiO<sub>3</sub> peak. The narrow rocking curve implies that the SrTiO<sub>3</sub> film on silicon possesses a low degree of mosaic spread along the out-of-plane direction. Note, as we discuss in more detail below, that the observation of a narrow 002 rocking curve peak only implies that the density of threading dislocations that are screw dislocations with out-of-plane line direction (or have screw component with out-of-plane line direction) in the SrTiO<sub>3</sub> film is low. The film could have high densities of threading dislocations that are pure edge dislocations with out-of-plane line direction as such dislocations will not cause broadening in the out-of-plane direction; this has been shown nicely in (0001) GaN films grown on (0001) Al<sub>2</sub>O<sub>3</sub> substrates, where rocking curve FWHM of the 0002 GaN peak were found to be 0.011° despite the presence of  $\sim 2 \times 10^{10} \text{ cm}^{-2}$  threading edge dislocations [49].

With a FWHM of only  $\sim 0.0054^\circ$ , the rocking curve in Fig. 3(b) is the narrowest 002 SrTiO<sub>3</sub> rocking curve among all SrTiO<sub>3</sub> films on silicon reported in the literature [27], including post-annealed SrTiO<sub>3</sub> films on silicon [50, 51]. It is even narrower than the 002 rocking curve of typical SrTiO<sub>3</sub> single crystals [35-38]. Figures 3(c) and 3(d) show a two-dimensional rocking curve of a 10 nm thick SrTiO<sub>3</sub> film on silicon and the corresponding reciprocal space map (RSM) around the 002 SrTiO<sub>3</sub> peak, respectively. The narrow spreading of the RSM is consistent with



the rocking curve measurement, corroborating the high crystalline perfection of the SrTiO<sub>3</sub> film along the out-of-plane direction. In addition to the lab XRD measurement, we confirmed the peak broadening of the same 10 nm thick SrTiO<sub>3</sub> film on silicon with synchrotron diffraction measurements. The RSM of the same sample measured at the Cornell High Energy Synchrotron Source (CHESS) agrees with the lab XRD measurement, as Fig. 3(e) shows. With our refined growth method, SrTiO<sub>3</sub> films as thin as 5 unit-cell-thick can be measured with a lab XRD. A  $\theta$ -2 $\theta$  scan of a 5 unit-cell-thick SrTiO<sub>3</sub> film on silicon and a rocking curve of the 002 SrTiO<sub>3</sub> peak of the same film are shown in Fig. S1(a) and S1(b) in the Supplemental Material[52].

To test whether the narrow FWHM of the 002 rocking curve (a symmetric peak) is indicative that the film has a low density of threading dislocations (as would follow from classic work in which the dislocations that broaden the rocking curve are assumed to be randomly distributed) [33], the rocking curve of an asymmetric peak was also measured. Figure 3(f) shows the rocking curve of the 103 SrTiO<sub>3</sub> peak and the 002 SrTiO<sub>3</sub> peak (with intensities normalized) measured on a 300 nm thick SrTiO<sub>3</sub> film on silicon. In contrast with the very narrow rocking curve of the 002 SrTiO<sub>3</sub> peak, the rocking curve of the 103 SrTiO<sub>3</sub> peak is ~8 times broader. This significant difference in rocking curve width is consistent with the defect microstructure revealed by STEM (described at the end of the manuscript). Specifically, it is consistent with the film containing a high density of threading dislocations and the narrow FWHM observed for the 002 peak is due to these threading dislocations being predominantly edge dislocations with out-of-plane line direction analogous to what was observed for some (0001) GaN films grown on (0001) Al<sub>2</sub>O<sub>3</sub> substrates [49].

XRD pole figure measurements sampling the 111 Si and 101 SrTiO<sub>3</sub> families of peaks of the same 20 nm thick SrTiO<sub>3</sub> on silicon characterized in Fig. 1 are shown in Fig. 3(g). The radial coordinate and the angular coordinate correspond to the XRD  $\chi$  angle and the  $\phi$  angle,

respectively. For the entire range ( $0^\circ < \chi < 90^\circ$ ,  $0^\circ < \phi < 360^\circ$ ) measured, only the 111 Si family of peaks ( $\chi = 54.73^\circ$ ,  $2\theta = 28.44^\circ$ ) and the 101 SrTiO<sub>3</sub> family of peaks ( $\chi = 45^\circ$ ,  $2\theta = 32.4^\circ$ ) were detected, indicating that the epitaxial relationship is: (001) Si  $\parallel$  (001) SrTiO<sub>3</sub>, [110] Si  $\parallel$  [100] SrTiO<sub>3</sub>.

The influence of the deposition temperature of the initial half monolayer of strontium on the bare silicon substrate on the crystalline quality (as judged by the FWHM of the 002 rocking curve) of the SrTiO<sub>3</sub> film was investigated by growing 20 nm thick SrTiO<sub>3</sub> films and depositing strontium at temperatures from  $\sim 200$  to  $\sim 850$  °C. To ensure a half a monolayer of strontium, the silicon was thermally cleaned rather than using strontium-assisted deoxidation [53]. This is because the latter method leaves a fractional monolayer of strontium atoms on the silicon surface after the strontium-assisted deoxidation. At each strontium deposition temperature, multiple 20 nm thick SrTiO<sub>3</sub> films were grown and the film with the narrowest FWHM of the rocking curve for each temperature was chosen for comparison. Figure 4(a) shows the smallest FWHM value of the 002 SrTiO<sub>3</sub> peak of 20 nm thick SrTiO<sub>3</sub> films obtained as a function of deposition temperature, indicating that 20 nm thick SrTiO<sub>3</sub> films with narrow rocking curves can be grown over a wide range of strontium deposition temperatures:  $\sim 200$  to  $\sim 800$  °C.

At a deposition temperature of  $\sim 850$  °C the rocking curve of the 002 SrTiO<sub>3</sub> peak is significantly broader. This might be due to the diffusion of strontium atoms into the bulk silicon substrate or evaporation from the surface of the substrate at such a high temperature. Either way the half monolayer strontium template for epitaxial SrTiO<sub>3</sub> growth would be incomplete. Even though the 002 rocking curve of the SrTiO<sub>3</sub> film is degraded when the half monolayer of strontium is deposited at  $\sim 850$  °C, a phase-pure 20 nm thick SrTiO<sub>3</sub> film with a  $\theta$ - $2\theta$  scan containing only  $00\ell$  Bragg reflections still results.

It was previously regarded as difficult or impossible to grow crystalline oxides on silicon when the half monolayer of strontium was deposited at low temperatures and a silicide layer was not formed, say at  $\sim 200$  or  $\sim 300$  °C [32]. Indeed earlier work utilized temperatures  $\geq 600$  °C for the deposition of the strontium on bare silicon prior to depositing  $\text{SrTiO}_3$  on top of it [15, 20, 22, 23, 54]. Although the RHEED patterns of the as-grown first 2.5 unit-cells of  $\text{SrTiO}_3$  are not sharp, we find (see Fig. S2 in the Supplemental Material[52]) that when the half a monolayer of strontium is deposited at  $\sim 200$  or  $\sim 300$  °C, after recrystallization in vacuum at  $\sim 580$  °C, the FWHM of the 002  $\text{SrTiO}_3$  rocking curves are comparable to that of the  $\text{SrTiO}_3$  films grown on a half monolayer of strontium deposited at higher temperatures. The XRD  $\theta$ - $2\theta$  scan and rocking curve of a 60 nm thick  $\text{SrTiO}_3$  with its half a monolayer of strontium deposited at  $\sim 300$  °C are shown in Fig. S3 in the Supplemental Material[52].

When the half monolayer of strontium is deposited at 850, 650, or 300 °C, it induces different (001) Si surface reconstructions, which can be shown by measuring the RHEED intensity of the half order streak along the [110] azimuth of (001) Si as a function of strontium coverage. Figure S4 in the Supplemental Material[52] shows this evolution for a half monolayer of strontium deposited at 850, 650, and 300 °C. Although the evolution of the RHEED intensity as a function of strontium coverage changes with substrate temperature, our growth results manifest unambiguously that a half monolayer of strontium can serve as a template for the growth of epitaxial  $\text{SrTiO}_3$  films on silicon with narrow 002  $\text{SrTiO}_3$  rocking curves no matter whether it forms the so-called silicide layer[20] or stays (partially) physisorbed to the silicon surface [32].

Prior reports show  $\text{SrTiO}_3$  films with a narrow 002  $\text{SrTiO}_3$  rocking curve on silicon for film thickness less than about 2 nm, where the  $\text{SrTiO}_3$  is commensurately strained to the underlying silicon substrate [6] or for film thicknesses above about 100 nm [17, 50, 55]. At intermediate

thicknesses the films show higher rocking curve FWHMs of the 002  $\text{SrTiO}_3$  peak. Such behavior is typical for the growth of mismatched epitaxial films [56]. Our work extends the thickness range over which films with narrow rocking curves are obtained from  $\sim 5$  unit-cells to  $\sim 300$  nm, as is shown in Fig. 4(b). A comparison with representative  $\text{SrTiO}_3$  films on silicon from the literature [6, 17] is included in Fig. 4(b). Raw data of the rocking curves of the 002  $\text{SrTiO}_3$  peak of  $\text{SrTiO}_3$  films of different thicknesses are shown in Fig. 4(c). Judging from the narrow rocking curve of the 002  $\text{SrTiO}_3$  peak, we believe that the half monolayer of strontium on silicon not only acts as a diffusion barrier for protecting the (001) Si surface from being oxidized during the initial  $\text{SrTiO}_3$  growth, but also influences the type of threading dislocations that subsequently form. In our case these threading dislocations are predominantly edge dislocations with out-of-plane line direction, which is consistent with the extremely narrow FWHM of the 002 rocking curves as well as the STEM results described below. The out-of-plane lattice parameter of the  $\text{SrTiO}_3$  films as a function of the film thickness is shown in Fig. 4(d), from which we see that the  $\text{SrTiO}_3$  film relaxes quickly after its thickness is above about 5 unit-cells.

Measurements of the rocking curves of the 003 and 004  $\text{SrTiO}_3$  peaks indicate that our  $\text{SrTiO}_3$  films on silicon of intermediate thicknesses such as 20 nm thick can be described by the unconventional mosaic crystal model [57]. To be specific, the diffuse or the broad tail of the rocking curve comes from the short-range order of independent scattering of individual dislocations, while the sharp peak seen from the 002  $\text{SrTiO}_3$  peak is due to the long-range correlation of the  $\text{SrTiO}_3$  film, and is not seen in higher order peaks such as the 003 and 004  $\text{SrTiO}_3$  peaks [57]. Figure S5 in the Supplemental Material[52] shows the rocking curves of the  $00\ell$   $\text{SrTiO}_3$  peaks ( $\ell = 1, 2, 3$ , and 4) of a 40 nm thick  $\text{SrTiO}_3$  film on silicon. Only the rocking curves of the 001 and 002  $\text{SrTiO}_3$  peaks are narrow; the same does not hold for the 003 and 004

SrTiO<sub>3</sub> peaks. This implies that the SrTiO<sub>3</sub> film on silicon is a so-called unconventional mosaic crystal [57].

We measured the azimuth rotational disorder of the SrTiO<sub>3</sub> films on silicon via XRD  $\phi$  scans. As an example, a 60 nm thick SrTiO<sub>3</sub> on silicon film shows a relatively large FWHM of  $\sim 0.75^\circ$  of the 101 SrTiO<sub>3</sub> peak for a  $\phi$  scan (Figure S6 in the Supplemental Material[52]), which implies relatively large in-plane mosaic spread. The rocking curve FWHM of the 002 SrTiO<sub>3</sub> peak of this same 60 nm thick film is  $\sim 0.012^\circ$ . The FWHM of azimuthal  $\phi$  scans as a function of the film thickness is shown in Fig. 4(e), indicating that the rotational disorder of the SrTiO<sub>3</sub> film decreases as the film thickness increases. The existence of a considerable amount of in-plane rotational disorder of SrTiO<sub>3</sub> films on silicon can be attributed to the lattice mismatch as well as the relatively large difference between the thermal expansion coefficient of silicon (averaging  $3.5 \times 10^{-6} \text{ K}^{-1}$  between room temperature and 520 °C) [58] and that of SrTiO<sub>3</sub> (averaging  $1.08 \times 10^{-5} \text{ K}^{-1}$  between room temperature and 520 °C) [58, 59]. The large difference between thermal expansion coefficients between the substrate and the film can introduce extra misfit between the film and the substrate, which can yield additional in-plane rotational disorder during the cool-down process after the film growth [60].

Cross-sectional high-angle annular dark field (HAADF) STEM was used to clarify the defect microstructure and characterize the interface between the SrTiO<sub>3</sub> and silicon. A representative image of the interface between a 10 nm thick SrTiO<sub>3</sub> film and silicon substrate is shown in Fig. 5(a). Although we used only the epitaxy-by-periodic-annealing method (with no high temperature growth step) to grow the SrTiO<sub>3</sub> film, we see an amorphous SiO<sub>2</sub> layer at the interface between the SrTiO<sub>3</sub> film and the silicon substrate. This oxidation of the surface of the

silicon either came from the diffusion of oxygen through the SrTiO<sub>3</sub> film during the ~300 °C deposition steps or more likely during the vacuum annealing step at 580 °C.

We also performed plan-view STEM to characterize the microstructure of our SrTiO<sub>3</sub> on silicon films. As is clearly visible in Fig. 5(b), the films show a high density of crystalline defects. While some of the defects can be easily identified by a simple Burgers circuit, as shown in Fig. 5(d), many others have a more complicated extended and branching structure, like the one shown in Fig. 5(c). By following the rows of strontium sites (yellow arrows) across the defect shown in Fig. 5(c), a clear out-of-phase boundary [61, 62] can be seen. Interestingly, the boundary shown here — as in many of the defects observed in these films — runs along the [110]  $a_{\text{SrTiO}_3}$  direction corresponding to an  $(a+b)/2$  unit cell shift. Towards the termination of the defect, the exact structure in the HAADF STEM image becomes less clear. Nonetheless, Fourier peak analysis suggests that the structure in this and similar regions can be well described by a combination of threading dislocations and out-of-phase boundaries, as shown in Figure S7 in the Supplemental Material[52].

The underlying cause of the out-of-phase boundaries could be the coalescence of nuclei or the incorporation of planar defects. Because the step height of silicon does not match that of SrTiO<sub>3</sub>, SrTiO<sub>3</sub> nuclei that form on different terraces of the silicon substrate will be out-of-phase with each other. When the growth fronts from such separate SrTiO<sub>3</sub> nuclei coalesce, out-of-phase boundaries can form [62]. Another possible nucleation mechanism is due to non-stoichiometry. If the SrTiO<sub>3</sub> is locally SrO-rich, an extra SrO rock salt layer could insert into the SrTiO<sub>3</sub> perovskite structure forming a Ruddlesden-Popper fault [63, 64]. These SrO double layers cause  $\frac{a}{2}$  [110] shifts in the position of the SrTiO<sub>3</sub> unit cells on either side of such a

crystallographic shear fault [65]. The resulting offset in coalescing SrTiO<sub>3</sub> growth fronts would again give rise to an out-of-phase boundary.

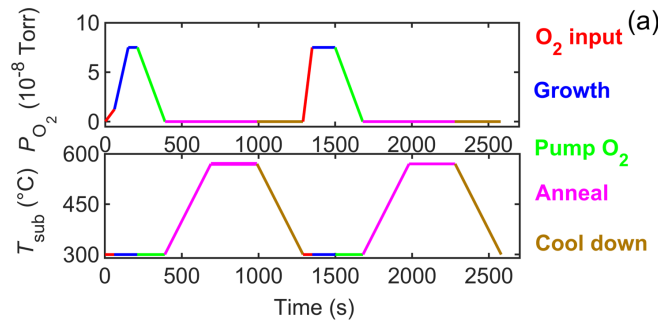
Employing the same Fourier peak analysis mentioned above, threading dislocations are easily identified and located throughout several plan-view STEM images to obtain a representative sampling. The SrTiO<sub>3</sub> films are found to contain a high density of threading dislocations,  $\sim 8 \times 10^{11} \text{ cm}^{-2}$ . The FWHM of the 002 rocking curve of the same film studied by STEM is  $\sim 0.008^\circ$ . Note that this density of threading dislocations is far higher than that found in typical SrTiO<sub>3</sub> single crystals, which lie in the  $(3 - 10) \times 10^5 \text{ cm}^{-2}$  range [39-41].

This massive difference in dislocation density begs the question of how it is possible for a SrTiO<sub>3</sub> film that contains a threading dislocation density more than six orders of magnitude higher than a SrTiO<sub>3</sub> single crystal to exhibit an 002 SrTiO<sub>3</sub> rocking curve with a FWHM ( $\sim 0.008^\circ$ ) that is considerably narrower than that of the single crystal? As shown in Fig. 5(d), the dominant Burgers vector is found to be  $[100] a_{\text{SrTiO}_3}$ . The threading dislocations are thus pure edge dislocations with out-of-plane line direction and the extremely narrow 002 rocking curves arise from the insensitivity of the 002 rocking curve to these pure edge dislocations, as has been reported previously for (0001) GaN / (0001) Al<sub>2</sub>O<sub>3</sub> films [49]. When dislocations are distributed anisotropically, as they are in these SrTiO<sub>3</sub>/Si films, it is insufficient to take a single narrow rocking curve peak as evidence of structural perfection. Assessing multiple peaks becomes important to establish the structural distortions present in multiple directions.

In summary, by depositing a half monolayer of strontium metal on bare (001) Si in the substrate temperature range 200 – 800 °C, in combination with a carefully controlled epitaxy-by-periodic-annealing method, we have lowered the out-of-plane mosaic spread of the SrTiO<sub>3</sub> films on silicon. SrTiO<sub>3</sub> films of low out-of-plane mosaic spread with thicknesses from 5 unit-cells to  $\sim 300 \text{ nm}$  were achieved. Our work establishes a well tested methodology for consistently

growing epitaxial SrTiO<sub>3</sub> films on silicon using MBE. This study has the potential of increasing the quality of not only the SrTiO<sub>3</sub> films on silicon, but also that of overlying epitaxial functional layers as the SrTiO<sub>3</sub> layer serves as an epitaxial template for the integration of oxides with a multitude of functional properties with silicon [66-68].

Z.W. and D.G.S. gratefully acknowledge the support from a GRO “functional oxides” project from the Samsung Advanced Institute of Technology. H.P. acknowledges support by the National Science Foundation [Platform for the Accelerated Realization, Analysis, and Discovery of Interface Materials (PARADIM)] under Cooperative Agreement No. DMR-1539918. B.H.G. and L.F.K. acknowledge support by the Department of Defense Air Force Office of Scientific Research (No. FA 9550-16-1-0305). Synchrotron-based x-ray experiment is conducted at the Cornell High Energy Synchrotron Source (CHESS) that is supported by the National Science Foundation under award DMR-1332208. This work made use of the Cornell Center for Materials Research (CCMR) Shared Facilities, which are supported through the NSF MRSEC program (No. DMR-1719875). The FEI Titan Themis 300 was acquired through No. NSF-MRI-1429155, with additional support from Cornell University, the Weill Institute, and the Kavli Institute at Cornell. Substrate preparation was performed in part at the Cornell NanoScale Facility, a member of the National Nanotechnology Coordinated Infrastructure (NNCI), which is supported by the NSF (Grant No. ECCS-15420819).





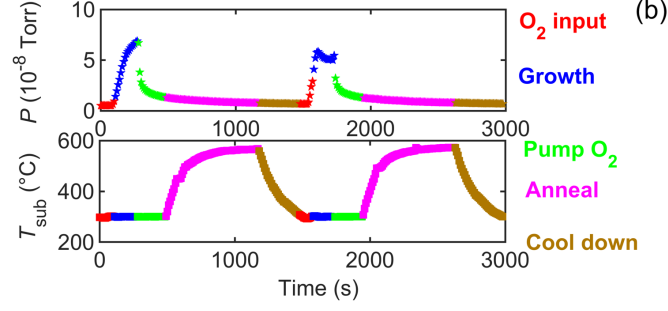


FIG. 1. (a) Schematic drawing of the growth pathway for the epitaxy-by-periodic-annealing method of the initial 5 unit-cells of  $\text{SrTiO}_3$  on silicon.  $T_{\text{sub}}$  is the substrate temperature and  $P_{\text{O}_2}$  is the oxygen partial pressure. Different colors indicate different stages. Note the difference of the  $\text{O}_2$  introduction ( $\text{O}_2$  input) step between the first 2.5 unit cells and the second 2.5 unit cells of  $\text{SrTiO}_3$  growth. (b) A set of actual growth parameters recorded during the growth of 5 unit-cells of  $\text{SrTiO}_3$  on silicon.  $P$  is the background oxygen partial pressure measured by the chamber ion gauge.  $T_{\text{sub}}$  is the substrate thermocouple temperature.

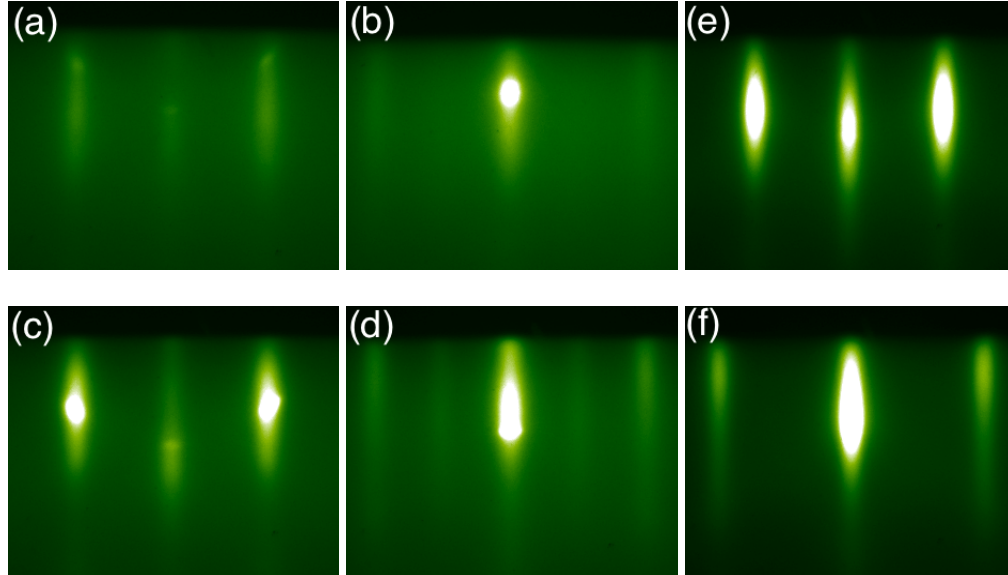


FIG. 2. RHEED images at different stages during the growth of the 20 nm thick  $\text{SrTiO}_3$  film on silicon. A half a monolayer of strontium was deposited at  $\sim 800^\circ\text{C}$ , followed by another half a monolayer of strontium deposited at  $\sim 300^\circ\text{C}$ . (a) The as-grown and (c) annealed first 2.5 unit cells of  $\text{SrTiO}_3$  viewed along the  $[100]$  azimuth of  $(001)$   $\text{SrTiO}_3$ . (b) The as-grown and (d) annealed first 2.5 unit cells of  $\text{SrTiO}_3$  viewed along the  $[110]$  azimuth of  $(001)$   $\text{SrTiO}_3$ .

SrTiO<sub>3</sub>. RHEED patterns after the growth of the 20 nm thick SrTiO<sub>3</sub> film viewed along (e) the [100] azimuth and (f) the [110] azimuth of (001) SrTiO<sub>3</sub>.

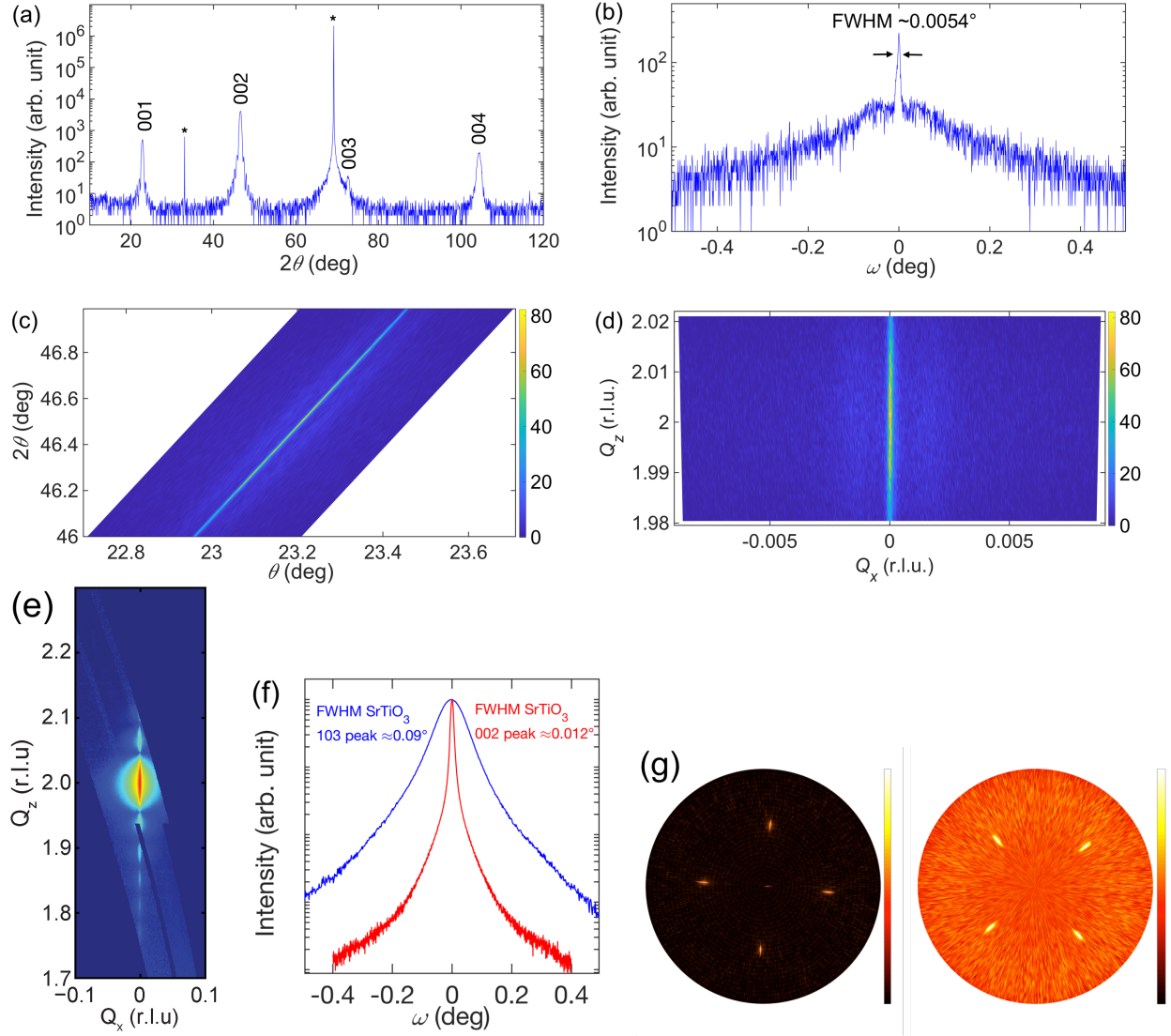
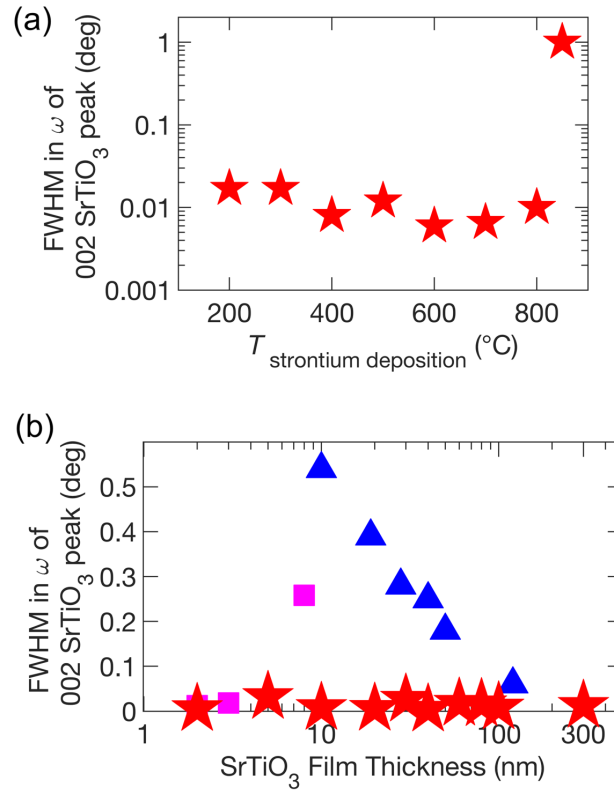


FIG. 3. XRD using (a – d, and f, g) laboratory and (e) sychrotron diffractometers of two SrTiO<sub>3</sub> films grown on silicon in this study. (a)  $\theta$ - $2\theta$  scan of the 20 nm thick SrTiO<sub>3</sub> on silicon shows only  $00\ell$  Bragg reflections, which in combination with the RHEED images indicates an epitaxial SrTiO<sub>3</sub> film on silicon. Asterisks indicate peaks arising from the silicon substrate. (b) Rocking curve of the 002 SrTiO<sub>3</sub> peak of the 20 nm thick SrTiO<sub>3</sub> on silicon has a FWHM of  $\sim 0.0054^\circ$ . (c) Rocking curves around the 002 SrTiO<sub>3</sub> peak of the 10 nm thick SrTiO<sub>3</sub> on silicon, along with (d) its corresponding RSM exhibit peak broadening consistent with the rocking curve. The broadening in the  $\theta$ - $2\theta$  scan (a) is caused by the finite thickness of the film, while the confinement along the  $\omega$  direction shows low mosaic spread in the out-of-plane direction. For the RSM, the broadening along the  $Q_z$  direction is due

to the finite thickness of the film, while the narrow width in the  $Q_x$  direction indicates the low mosaic spread of the  $\text{SrTiO}_3$  film in this direction. (e) The RSM of the 10 nm thick  $\text{SrTiO}_3$  on silicon with clear thickness fringes measured at the G2 station of CHESS indicates that the narrow intensity spread along the  $Q_x$  direction and the broadening along the  $Q_z$  direction are consistent with the lab XRD measurement. (f) Rocking curves of the 103 and 002  $\text{SrTiO}_3$  peaks of the 300 nm thick  $\text{SrTiO}_3$  film on silicon. (g) XRD pole figure measurements sampling the 202 Si and 101  $\text{SrTiO}_3$  family of peaks of the 20 nm thick  $\text{SrTiO}_3$  on silicon. The intensity color scale is logarithmic.



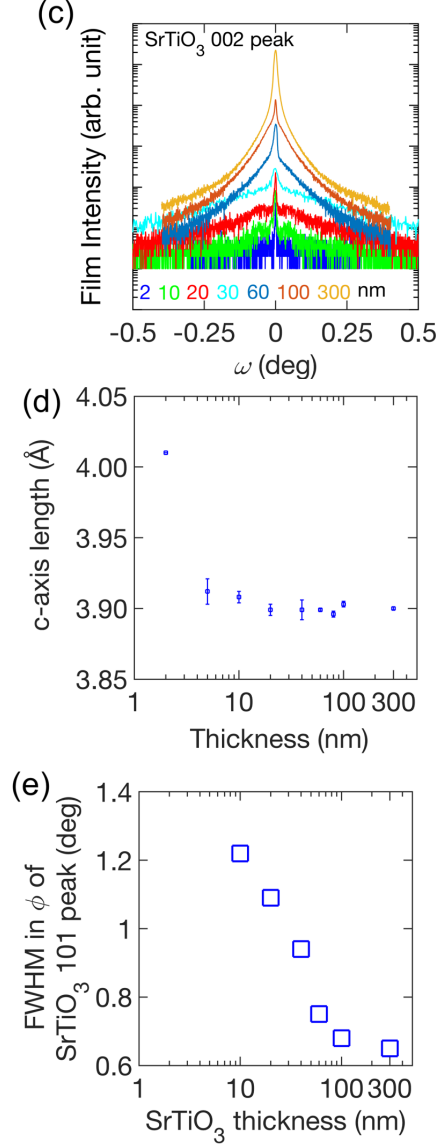


FIG. 4. (a) The rocking curve FWHMs of 20 nm thick films of SrTiO<sub>3</sub> on silicon as a function of the temperature ( $T_{\text{strontium deposition}}$ ) at which the half a monolayer of strontium was deposited shows that 20 nm thick SrTiO<sub>3</sub> films with narrow rocking curves can be grown when the half a monolayer of strontium is deposited anywhere in the  $\sim 200$  to  $800$  °C range. Rocking curves of the 002 SrTiO<sub>3</sub> peak were measured. All data points are from 20 nm thick SrTiO<sub>3</sub> films grown on silicon with  $\theta$ - $2\theta$  scans showing only  $00\ell$  Bragg reflections. (b) FWHMs of SrTiO<sub>3</sub> films of different thicknesses on silicon show that from  $\sim 2$  to  $\sim 300$  nm, our growth method yielded films with narrow FWHM. The data points of this work are represented with red stars. The purple data points and blue data points are from Ref. 6, and 54, respectively. (c) Raw data of the rocking curves of the 002 SrTiO<sub>3</sub> peak of SrTiO<sub>3</sub> films of different thicknesses. (d) Out-of-plane lattice parameter of the SrTiO<sub>3</sub> film on silicon as a function of film

thickness showing that the SrTiO<sub>3</sub> film on silicon relaxes quickly above a film thickness of about 5 unit cells. (e) The FWHM of the 101 SrTiO<sub>3</sub> peak in  $\phi$  (measured in a triple axis geometry) for SrTiO<sub>3</sub> films on silicon as a function of film thickness indicates that the SrTiO<sub>3</sub> films on silicon possess a relatively large in-plane rotational disorder, and the in-plane mosaicity spread decreases as film thickness increases.

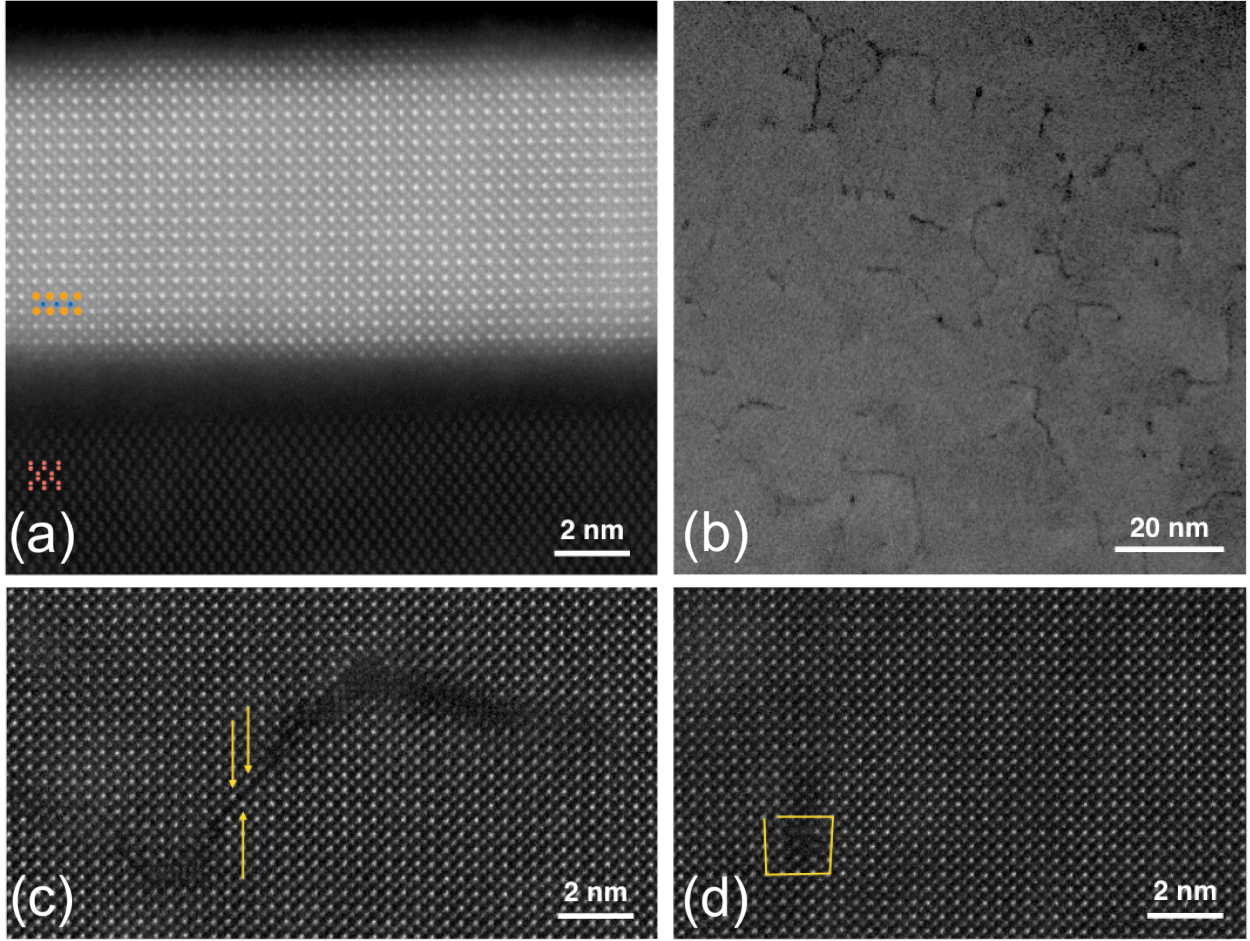


FIG. 5. (a) STEM images of a 10 nm thick SrTiO<sub>3</sub> film on silicon. The interfacial region has an amorphous SiO<sub>2</sub> layer. Strontium (orange), titanium (blue), and silicon (red) atoms are overlaid to show the schematic atomic structure. (b) Plan-view STEM image of a 20 nm thick SrTiO<sub>3</sub> film on silicon showing a variety of both localized and branching dislocations with a density of  $\sim 8 \times 10^{11} \text{ cm}^{-2}$ , between which exist crystallographically defect-free regions with area on the order of  $\sim (20 \text{ nm})^2$ . (c) Atomic resolution STEM image of a branching defect like those seen in (b), with an out-of-phase boundary highlighted by yellow arrows marking rows of bright strontium atoms

offset on either side of the fault. (d) Atomic resolution STEM image of a localized edge dislocation like those seen in (b) with a Burgers circuit shown in yellow.

## Reference:

- 1 H. Mori, and H. Ishiware, [Jpn. J. Appl. Phys. \*\*30\*\*, L1415 \(1991\).](#)
- 2 S. H. Baek, and C. B. Eom, [Acta Mater. \*\*61\*\*, 2734 \(2013\).](#)
- 3 S. A. Chambers, Y. Liang, Z. Yu, R. Droopad, J. Ramdani, and K. Eisenbeiser, [Appl. Phys. Lett. \*\*77\*\*, 1662 \(2000\).](#)
- 4 Y. Wang, C. Ganpule, B. T. Liu, H. Li, K. Mori, B. Hill, M. Wuttig, R. Ramesh, J. Finder, Z. Yu, R. Droopad, and K. Eisenbeiser, [Appl. Phys. Lett. \*\*80\*\*, 97 \(2002\).](#)
- 5 T. Eisuke, I. Kensuke, M. Bum-Ki, and I. Hiroshi, [Jpn. J. Appl. Phys. \*\*34\*\*, 5202 \(1995\).](#)
- 6 M. P. Warusawithana, C. Cen, C. R. Sleasman, J. C. Woicik, Y. Li, L. F. Kourkoutis, J. A. Klug, H. Li, P. Ryan, L. P. Wang, M. Bedzyk, D. A. Muller, L. Q. Chen, J. Levy, and D. G. Schlom, [Science \*\*324\*\*, 367 \(2009\).](#)
- 7 M. Belmeguenai, S. Mercone, C. Adamo, L. Méchin, C. Fur, P. Monod, P. Moch, and D. G. Schlom, [Phys. Rev. B \*\*81\*\*, 054410 \(2010\).](#)
- 8 L. Méchin, C. Adamo, S. Wu, B. Guillet, S. Lebargy, C. Fur, J.-M. Routoure, S. Mercone, M. Belmeguenai, and D. G. Schlom, [Phys. Status Solidi A, \*\*209\*\*, 1090 \(2012\).](#)
- 9 J. Wang, H. Zheng, Z. Ma, S. Prasertchoung, M. Wuttig, R. Droopad, J. Yu, K. Eisenbeiser, and R. Ramesh, [Appl. Phys. Lett. \*\*85\*\*, 2574 \(2004\).](#)
- 10 S. H. Baek, J. Park, D. M. Kim, V. A. Aksyuk, R. R. Das, S. D. Bu, D. A. Felker, J. Lettieri, V. Vaithyanathan, S. S. N. Bharadwaja, N. Bassiri-Gharb, Y. B. Chen, H. P. Sun, C. M. Folkman, H. W. Jang, D. J. Kreft, S. K. Sterriffer, R. Ramesh, X. Q. Pan, S. Trolier-McKinstry, D. G. Schlom, M. S. Rzechowski, R. H. Blick, and C. B. Eom, [Science \*\*334\*\*, 958 \(2011\).](#)
- 11 U. K. Bhaskar, N. Banerjee, A. Abdollahi, Z. Wang, D. G. Schlom, G. Rijnders, and G. Catalan, [Nat. Nanotechnol. \*\*11\*\*, 263 \(2016\).](#)
- 12 H. Ishiware, N. Tsuji, H. Mori, and H. Nohira, [Appl. Phys. Lett. \*\*61\*\*, 1459 \(1992\).](#)
- 13 S. Abel, T. Stöferle, C. Marchiori, C. Rossel, M. D. Rossell, R. Erni, D. Caimi, M. Sousa, A. Chelnokov, B. J. Offrein, and J. Fompeyrine, [Nat. Commun. \*\*4\*\*, 1671 \(2013\).](#)
- 14 J. W. Park, D. F. Bogorin, C. Cen, D. A. Felker, Y. Zhang, C. T. Nelon, C. W. Bark, C. M. Folkman, X. Q. Pan, M. S. Rzechowski, J. Levy, and C. B. Eom, [Nat. Commun. \*\*1\*\*, 94 \(2010\).](#)
- 15 E. N. Jin, L. Kornblum, D. P. Kumah, K. Zou, C. C. Broadbridge, J. H. Ngai, C. H. Ahn, and F. J. Walker, [APL Mater. \*\*2\*\*, 116109 \(2014\).](#)
- 16 L. Ji, M. D. McDaniel, S. J. Wang, A. B. Posadas, X. H. Li, H. Y. Huang, J. C. Lee, A. A. Demkov, A. J. Bard, J. G. Ekerdt, and E. T. Yu, [Nat. Nanotechnol. \*\*10\*\*, 84 \(2015\).](#)
- 17 X. Gu, D. Lubyshev, J. Batzel, J. M. Fastenau, W. K. Liu, R. Pelzel, J. F. Magana, Q. Ma, and V. R. Rao, [J. Vac. Sci. Technol., B \*\*28\*\*, C3A12 \(2010\).](#)
- 18 L. Zhang, and R. Engel-Herbert, [Phys. Status Solidi RRL \*\*8\*\*, 917 \(2014\).](#)



- 19 C. Guguschev, Z. Galazka, D. J. Kok, U. Juda, A. Kwasniewski, and R. Uecker, [CrystEngComm](#) **17**, 4662 (2015).
- 20 R. A. McKee, F. J. Walker, and M. F. Chisholm, [Phys. Rev. Lett.](#) **81**, 3014 (1998).
- 21 H. Li, X. Hu, Y. Wei, Z. Yu, X. Zhang, R. Droopad, A. A. Demkov, J. Edwards, K. Moore, W. Ooms, J. Kulik, and P. Fejes, [J. Appl. Phys.](#) **93**, 4521 (2003).
- 22 Z. Yu, J. Ramdani, J. A. Curless, C. D. Overgaard, J. M. Finder, R. Droopad, K. W. Eisenbeiser, J. A. Hallmark, W. J. Ooms, and V. S. Kaushik, [J. Vac. Sci. Technol., B](#) **18**, 2139 (2000).
- 23 Z. Yu, Y. Liang, C. Overgaard, X. Hu, J. Curless, H. Li, Y. Wei, B. Craigo, D. Jordan, R. Droopad, J. Finder, K. Eisenbeiser, D. Marshall, K. Moore, J. Kulik, and P. Fejes, [Thin Solid Films](#) **462-463**, 51 (2004).
- 24 F. J. Walker, and R. A. McKee, [High Dielectric Constant Materials: VLSI MOSFET Applications](#), (Springer, 2005), page. 607.
- 25 X. Y. Zhou, J. Miao, J. Y. Dai, H. L. W. Chan, C. L. Choy, Y. Wang, and Q. Li, [Appl. Phys. Lett.](#) **90**, 012902 (2007).
- 26 J. W. Reiner, A. M. Kolpak, Y. Segal, K. F. Garrity, S. Ismail-Beigi, C. H. Ahn, and F. J. Walker, [Adv. Mater.](#) **22**, 2919 (2010).
- 27 A. A. Demkov, and A. B. Posadas, [Integration of Functional Oxides with Semiconductors](#), (Springer New York, 2014), page. 115-158.
- 28 D. G. Schlom, [APL Mater.](#) **3**, 062403 (2015).
- 29 J. Lettieri, J. H. Haeni, and D. G. Schlom, [J. Vac. Sci. Technol., A](#) **20**, 1332 (2002).
- 30 C. J. Forst, C. R. Ashman, K. Schwarz, and P. E. Blochl, [Nature](#) **427**, 53 (2004).
- 31 L. F. Kourkoutis, C. S. Hellberg, V. Vaithyanathan, H. Li, M. K. Parker, K. E. Andersen, D. G. Schlom, and D. A. Muller, [Phys. Rev. Lett.](#) **100**, 036101 (2008).
- 32 J. W. Reiner, K. F. Garrity, F. J. Walker, S. Ismail-Beigi, and C. H. Ahn, [Phys. Rev. Lett.](#) **101**, 105503 (2008).
- 33 P. Gay, P. B. Hirsch, and A. Kelly, [Acta Metall.](#) **1**, 315 (1953).
- 34 J. Als-Nielsen and D. McMorrow, [Elements of Modern X-ray Physics](#), (John Wiley & Sons, 2011)
- 35 H. J. Scheel, J. G. Bednorz, and P. Dill, [Ferroelectrics](#) **13**, 507 (1976).
- 36 S. B. Qadri, J. S. Horwitz, D. B. Chrisey, R. C. Y. Auyeung, K. S. Grabowski, [Appl. Phys. Lett.](#) **66**, 1605 (1995).
- 37 P. I. Nabokin, D. Souptel, A. M. Balbashov, [J. Crys. Growth](#) **250**, 397 (2003).
- 38 M. D. Biegalski, D. D. Fong, J. A. Eastman, P. H. Fuoss, S. K. Streiffer, T. Heeg, J. Schubert, W. Tian, C. T. Nelson, X. Q. Pan, M. E. Hawley, M. Bernhagen, P. Reiche, R. Uecker, S. Trolier-McKinstry, and D. G. Schlom, [J. Appl. Phys.](#) **104**, 114109 (2008).
- 39 W. H. Rhodes, and W. D. Kingery, [J. Am. Ceram. Soc.](#) **49**, 521 (1966).
- 40 J. G. Bednorz, and H. J. Scheel, [J. Crys. Growth](#) **41**, 5 (1977).
- 41 C. Gerber, D. Anselmetti, J. G. Bednorz, J. Mannhart, and D. G. Schlom, [Nature](#) **350**, 279 (1991).
- 42 C. D. Theis, and D. G. Schlom, [J. Vac. Sci. Technol., A](#) **14**, 2677 (1996).
- 43 J. H. Haeni, C. D. Theis, and D. G. Schlom, [J. Electroceram.](#) **4**, 385 (2000).
- 44 C. M. Brooks, L. F. Kourkoutis, T. Heeg, J. Schubert, D. A. Muller, and D. G. Schlom, [Appl. Phys. Lett.](#) **94**, 162905 (2009).
- 45 G. Niu, G. Saint-Girons, B. Vilquin, G. Delhaye, J.-L. Maurice, C. Botella, Y. Robach, and G. Hollinger, [Appl. Phys. Lett.](#) **95**, 062902 (2009).

- 46 G. Niu, J. Penuelas, L. Largeau, B. Vilquin, J. L. Maurice, C. Botella, G. Hollinger, and G. Saint-Girons, [Phys. Rev. B \*\*83\*\*, 054105 \(2011\)](#).
- 47 G. Saint-Girons, R. Bachelet, R. Moalla, B. Meunier, L. Louahadj, B. Canut, A. Carretero-Genevriar, J. Gazquez, P. Regreny, C. Botella, J. Penuelas, M. G. Silly, F. Sirotti, and G. Grenet, [Chem. Mater. \*\*28\*\*, 5347 \(2016\)](#).
- 48 J. Lettieri, [PhD Thesis, Pennsylvania State University 2002](#).
- 49 B. Heying, X. H. Wu, S. Keller, Y. Li, D. Kapolnek, B. P. Keller, S. P. DenBaars, and J. S. Speck, [Appl. Phys. Lett. \*\*68\*\*, 643 \(1996\)](#).
- 50 J. W. Park, S. H. Baek, C. W. Bark, M. D. Biegalski, and C. B. Eom, [Appl. Phys. Lett. \*\*95\*\*, 061902 \(2009\)](#).
- 51 L. Zhang, Y. Wang, and R. Engel-Herbert, [J. Appl. Phys. \*\*119\*\*, 045301 \(2016\)](#).
- 52 See Supplemental Material at [] for extra XRD, RHEED, and STEM characterization of the SrTiO<sub>3</sub> films on silicon.
- 53 Y. Wei, X. Hu, Y. Liang, D. C. Jordan, B. Craigo, R. Droopad, Z. Yu, A. Demkov, J. L. Edwards, and W. J. Ooms, [J. Vac. Sci. Technol., B \*\*20\*\*, 1402 \(2002\)](#).
- 54 J. Sanghun, F. J. Walker, C. A. Billman, R. A. McKee, and H. Hwang, [IEEE Electron Device Lett. \*\*24\*\*, 218 \(2003\)](#).
- 55 X. Gu, D. Lubyshev, J. Batzel, J. M. Fastenau, W. K. Liu, R. Pelzel, J. F. Magana, Q. Ma, L. P. Wang, P. Zhang, and V. R. Rao, [J. Vac. Sci. Technol., B \*\*27\*\*, 1195 \(2009\)](#).
- 56 J. W. Matthews, [Surf. Sci. \*\*31\*\*, 241 \(1972\)](#).
- 57 P. F. Miceli, and C. J. Palmström, [Phys. Rev. B \*\*51\*\*, 5506 \(1995\)](#).
- 58 Y. S. Touloukian, R. Kirby, E. Taylor, and T. Lee, [Plenum, New York, 1977](#), page. 570.
- 59 D. de Ligny, and P. Richet, [Phys. Rev. B \*\*53\*\*, 3013 \(1996\)](#).
- 60 J. W. Matthews, [Epitaxial Growth, \(Academic Press, 1975\), page. 559-609](#).
- 61 J. M. Cowley, [Physical Review \*\*138\*\*, A1384 \(1965\)](#).
- 62 M. A. Zurbuchen, W. Tian, X. Q. Pan, D. Fong, S. K. Streiffer, M. E. Hawley, J. Lettieri, Y. Jia, G. Asayama, S. J. Fulk, D. J. Comstock, S. Knapp, A. H. Carim, D. G. Schlom, [J. Mater. Res. \*\*22\*\*, 1439 \(2007\)](#).
- 63 S. N. Ruddlesden, and P. Popper, [Acta Crystallogr. \*\*10\*\*, 538 \(1957\)](#).
- 64 S. N. Ruddlesden, and P. Popper, [Acta Crystallogr. \*\*11\*\*, 54 \(1958\)](#).
- 65 S. Andersson, and A. D. Wadsley, [Nature \*\*211\*\*, 581 \(1966\)](#).
- 66 Z. Wang, Z. Chen, A. B. Mei, X. Bai, D. A. Muller, and D. G. Schlom, [J. Vac. Sci. Technol., A \*\*36\*\*, 021507 \(2018\)](#).
- 67 Z. Wang, H. P. Nair, G. C. Correa, J. Jeong, K. Lee, E. S. Kim, A. Seidner H., C. S. Lee, H. J. Lim, D. A. Muller, and D. G. Schlom, [APL Materials \*\*6\*\*, 086101 \(2018\)](#).
- 68 Z. Wang, H. Paik, Z. Chen, D. A. Muller, and D. G. Schlom, [APL Materials \*\*7\*\*, 022520 \(2019\)](#).



